Bulletin of the Seismological Society of America, Vol. XX, No. XX, pp. –, – 2018, doi: 10.1785/0120180100

The 19 September 2017 M 7.1 Puebla-Morelos Earthquake: Spectral Ratios Confirm Mexico City Zoning

by Mehmet Çelebi, Valerie J. Sahakian,* Diego Melgar, and Luis Quintanar

Abstract One important element of understanding basin response to strong shaking is the analysis of spectral ratios, which may provide information about the dominant frequency of ground motion at specific locations. Spectral ratios computed from accelerations recorded by strong-motion stations in Mexico City during the mainshock of the 19 September 2017 **M** 7.1 Puebla-Morelos earthquake reveal predominate periods consistent with those mapped in the 2004 Mexican seismic design code. Furthermore, the predominant periods thus computed validate those studies using mainshock and aftershock recordings of the handful strong-motion stations that recorded the 19 September 1985 **M** 8.1 Michoacán earthquake. Even though the number of stations in each of the zones (zones I, II, IIIa, b, c, and d) is not the same, they still allow confirmation of site frequencies (periods) attributable to the specific zones (particularly those in zones IIIa, b, c, and d). Spectral ratios are computed with two different methods: (1) horizontal to horizontal (H/H) ratio of smoothed amplitude spectrum of a horizontal channel in direction X of a station with respect to the smoothed amplitude spectrum of the horizontal channel in the same X direction of a reference stiff soil (or rock) station and (2) horizontal to vertical (H/V) ratio (or also known as the Nakamura method) of both horizontal (H) and vertical (V) channels of the same station. We show a comparison of the identified frequencies (periods) derived by both methods and find they are very similar and in good agreement with those indicated in the zoning maps of Mexico City in the 2004 seismic design code.

Introduction

On 19 September 2017, the **M** 7.1 Puebla-Morelos earthquake occurred at 18:14:40 GMT (13:14:40 local time) at epicentral coordinates: latitude 18.40° N and longitude 98.72° W and depth of 57 km (The National Seismological Service of Mexico [SSN]). The U.S. Geological Survey (USGS) gave the epicentral coordinates as 18.5838° N and 98.3993° W and depth as 51 km (see Data and Resources). Geotechnical Extreme Events Reconnaissance (GEER) describes the earthquake as occurring "in a complex region of normal and reverse faults with a regional tectonic mechanism associated with the subduction of the Cocos plate under the North American plate. The epicenter was located 12 km southeast of the city of Axochiapan in the State of Morelos. As expected, there was no surface expression of the fault rupture reported by any of the reconnaissance teams dispatched to the area" (Geotechnical Extreme Events Reconnaissance [GEER], 2017). A recent inversion study by Melgar *et al.* (2018) indicates a northward dip. Additional information on the seismological aspects, tectonics, intensity, and ShakeMaps related to this event can be found at the USGS website.

A Note on 1985 and 2017 Earthquakes

It is well known that previous earthquakes occurring at far distances from Mexico City have caused significant loss of lives and extensive damage within the city. One of the most well known of such events was the 19 September 1985 **M** 8.1 Michoacán earthquake (Anderson *et al.*, 1986; Çelebi *et al.*, 1987a,b; Stone *et al.*, 1987). At an epicentral distance of ~400 km, this distant event caused 4287 casualties and 5728 buildings to either collapse or sustain heavy damage (Çelebi *et al.*, 1987a,b; Stone *et al.*, 1987). Relative locations of the 1985 and 2017 earthquake epicenters and epicentral distances from Mexico City are shown in Figure 1. We note that although the epicenter of the 1985 earthquake was farther away from Mexico City than the 2017 Puebla-Morelos event, it was an order of magnitude larger.

One of the main reasons that Mexico City sustain extensive damage from earthquakes that originate at far distances is that it is densely built on a filled lakebed (GEER, 2017).

*Also at Department of Earth Sciences, University of Oregon, Eugene, Oregon 97403.

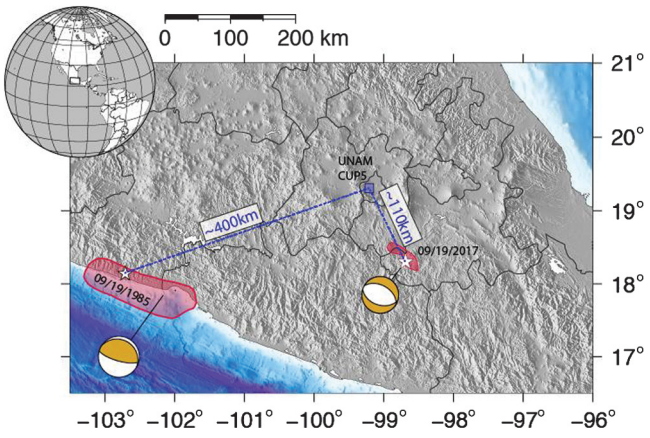

Figure 1. Relative locations of the 1985 and 2017 earthquakes with respect to Mexico City. Coordinates (latitudes and longitudes) of the epicenters of both 1985 and 2017 events are also indicated. The red shaded areas are rupture regions (from Mendoza and Hartzell, 1989, and Melgar *et al.*, 2018).

Hence, seismic design codes in Mexico recognize the site-specific zonation issues in Mexico City. The design codes have considered three zones that realistically represent lakebed areas as riskier. For example, at the time of the 1985 earthquake, the seismic zoning map used in design codes consisted of only three zones (hills [now zone I], transition [now zone II], and lake zone [now zone III]) (Fig. 2) (Çelebi *et al.*, 1987a). This older zonation map depicts not only limited number of the current key strong-motion stations but also includes locations of temporary stations established in 1985 earthquake-related aftershock studies (Çelebi *et al.*, 1987a) that are not repeated herein.

After the 1985 earthquake, several research groups focused on analyzing the seismic records, local geological structure, possible models, influence of Trans-Mexican volcanic belt, and generation and propagation of surface waves, as well as the role of the path between the source and the valley. A comprehensive literature review of this research is described in the work of Flores-Estrella *et al.* (2007).

Even though the amplification of seismic waves in the Valley of Mexico has been widely explained by local and regional soil properties (Sánchez-Sesma *et al.*, 1988; Shapiro *et al.*, 1997) or by the differences of quality factors of propagation of seismic waves at certain frequency-band windows (Iida and Kawase, 2004), the long-lasting duration of observed long-period strong motions inside the lake zone is a subject still under discussion and actively researched. Examples of such studies are by Chávez-García and Bard (1994) and Bard and Bouchon (1980). Kawase (2003), by analyzing 2D basin models, concluded that surface wavetrains generated at basin edges sustain rapid decay as they propagate and suggested discarding this mechanism as a possible explanation for the long seismic records. Singh and Ordaz (1993) explained the long-lasting duration of seismic signals in the valley as caused by regional-scale effects, such as the presence of scatterers around the basin that produce multipaths

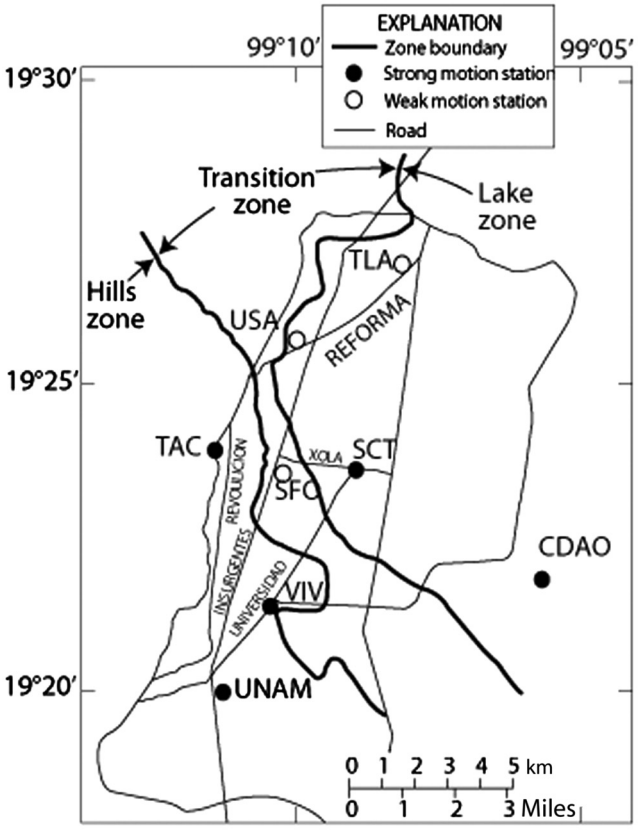

Figure 2. Zoning map of Mexico City that was in effect in 1985 (Çelebi *et al.*, 1987a). Solid lines are major avenues, and thick solid lines are boundaries of zones. Stations included in the study are marked with circles.

within the larger Valley of Mexico. Another explanation is that the interaction between incident wavefields and local basin conditions could produce elongation of the signal duration by means of coupling valley resonant frequencies with dominant periods of seismic waves (Chávez-García and Salazar, 2002).

More recently, Cruz-Atienza *et al.* (2016) simulated wavefield propagation in the Valley of Mexico, showing that deep structure provides conditions for a dominance of wave overtones on ground motion in the lake zone and that this propagation regime strongly contributes to the elongation of intense shaking at frequencies for which the largest amplification is observed.

In addition, significant studies of natural site period distribution across Mexico City (after the 1985 earthquake) were carried out by Lermo and Chávez-García (1993, 1994). The best-known result of these studies was a map of period contours in the Mexico basin. It is important to note that in this study, we show that spectral ratios computed using accelerations recorded at multiple stations in Mexico City during the 19 September 2017 earthquake allow identification of site frequencies (periods) that agree with those indicated by the 2004 seismic design code zoning maps of Mexico City.

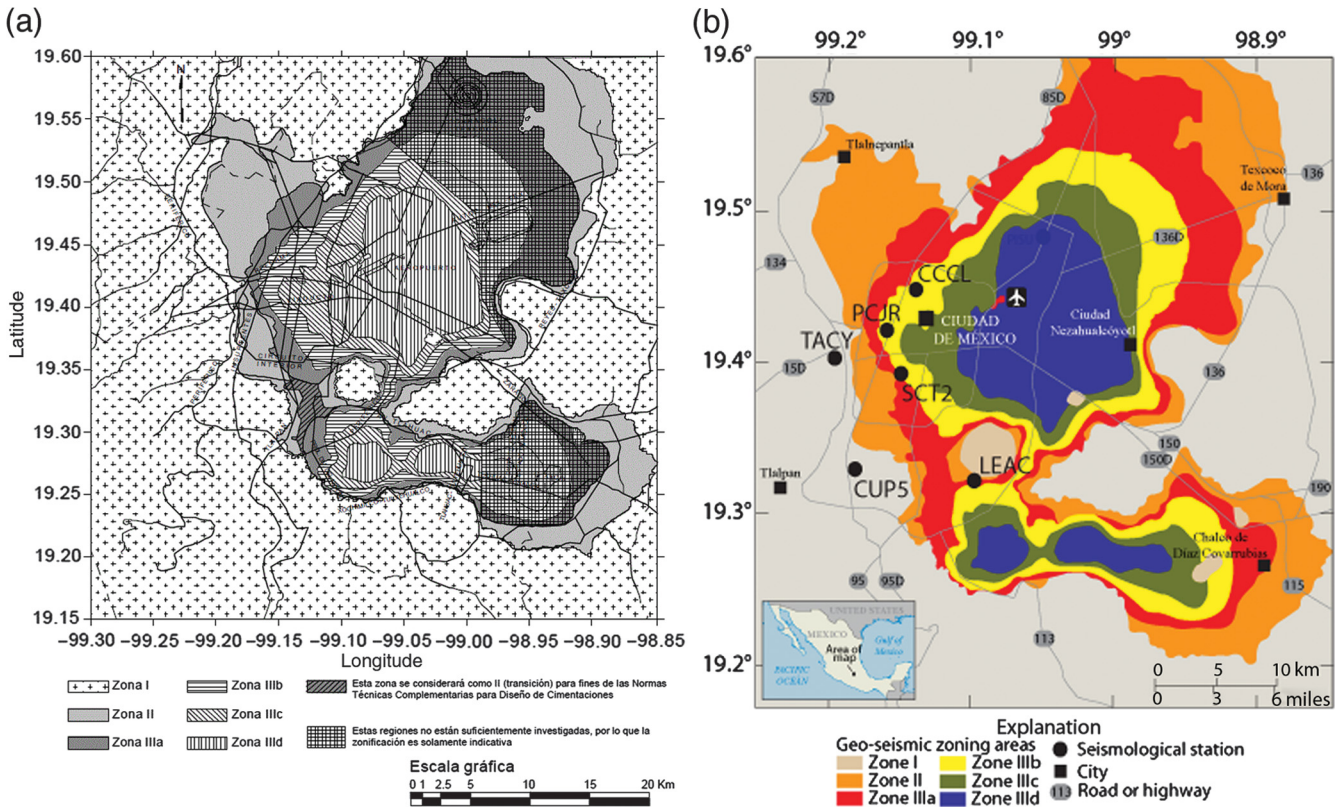

Figure 3. (a) Seismic zoning map in effect in 2017 in Mexico City (adopted from the Mexican seismic design code of 2004). Compared wth the 1985 zoning map, this map is far more detailed (zones denoted as zona; escala gráfica denotes the map scale). (b) 2017 zoning map modified from the 2004 Mexican seismic design code. Here, we use color to emphasize the different seismic zones and include some of the stations that recorded the 19 September 2017 **M** 7.1 earthquake. Station CUP5 used in this article is in close proximity to Universidad Nacional Autonoma de Mexico (UNAM) station that was the major reference station used in studies after the 19 September 1985 **M** 8.1 Michoacán earthquake (Çelebi *et al.*, 1987a). The inset in (b) depicts location of Mexico City within the Map of Mexico.

Naturally, during the past three decades since the 1985 event, Mexico City seismic zonation maps have evolved. The current seismic code further divides the lake zone (now zone III) into four subzones. Figure 3a shows the current seismic zoning map of Mexico City that has been in effect since 2004 (Mexican Seismic Design Code, 2004). Four subzones (a, b, c, and d) on the lake zone (zone III) are depicted in this map. Figure 3b shows a colored zoning map modified from the 2004 Mexican seismic design code. It includes some of the stations in different zones that recorded the 19 September 2017 **M** 7.1 earthquake. Station CUP5, used in this study, is in close proximity to Universidad Nacional Autonoma de Mexico (UNAM) station that was the major reference station used in studies conducted after the 19 September 1985 **M** 8.1 Michoacán earthquake (Çelebi *et al.*, 1987a).

Recently, Arroyo *et al.* (2013) evaluated the change in dominant periods in the lake zone of Mexico City. They studied the changes produced by ground subsidence through the use of site amplification factors and proposed an updated map for inclusion in the revisions to the 2004 seismic design code of Mexico. GEER (2017) cites this study and a UNAM-GEER study after the 2017 earthquake that confirmed the findings of Arroyo *et al.* (2013).

Accelerations recorded in Mexico City during both the 1985 and 2017 earthquakes were not large (mostly $<0.25g$). Table 1 shows a comparison of peak accelerations recorded in some of the stations that existed in 1985 as well as those

Table 1
Representative Number of Peak Accelerations during the 1985 and 2017 Mainshocks

		1985 Peak Acceleration (g)*		2017 Peak Acceleration (g)†	
	Zone	North–South	East–West	North–South	East–West
UNAM	I	0.03	0.035	0.046‡	0.055‡
CUP5	I	–	–	0.05	0.06
TACY	I	0.03	0.03	0.06	0.06
VIV	III	0.049	0.024		
JC84	II	–	–	0.22	0.21
CH84	II	–	–	0.15	0.23
SI53	IIIa	–	–	0.13	0.18
SCT	IIIb	0.098	0.168		
SCT2	IIIb			0.09	0.09

Zone designations are according to the current zoning map in the 2004 seismic design code. UNAM, Universidad Nacional Autonoma de Mexico.
*NIST report (Stone *et al.*, 1987).
†GEER report (2017).
‡Center for Engineering Strong Motion Data (see Data and Resources).

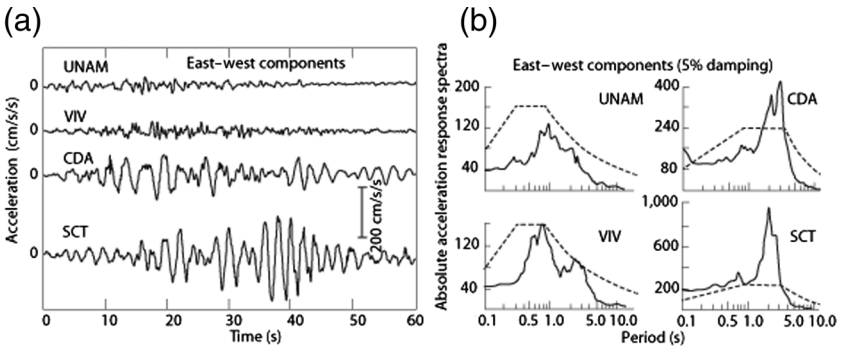

Figure 4. (a) Acceleration time histories for the 1985 mainshock at different locations in Mexico City compared with UNAM station. (b) Response spectra of the accelerations also depict the site amplifications. Design response spectrum in effect in 1985 is superimposed as dashed lines on each spectrum to facilitate comparison. (Adapted and redrawn with permission from the author, J. Anderson [9 April 2018] and reprinted with permission from American Association for the Advancement of Science [AAAS].)

Figure 5. Photos of the damaged Secretaria de Comunicaciones y Transportes (SCT, Ministry of Telecommunications and Transportation) building after the 1985 earthquake. It was severely damaged with several collapsed floors (see USGS Photographic Library website in Data and Resources).

during the recent 2017 event. In 1985, because there were a limited number of strong-motion stations, some larger peak accelerations probably occurred but were not recorded. Nonetheless, considering the reported damages caused by the 1985 or 1987 events, the level of peak accelerations was not the main cause of damage. As strongly evidenced by previous studies of the 1985 event, the frequency content and resulting resonating amplifications of ground motions were the main culprits leading to structural damage (Anderson *et al.*, 1986; Çelebi *et al.*, 1987a; Stone *et al.*, 1987).

Relevant to this study and for comparison later, amplifications of motions in the lake zone (the dubbed culprit during the 1985 event) are best displayed by the now well-known acceleration time history and corresponding response spectra plots. In 1985, the strong-motion stations that existed were UNAM and TAC in the hills zone; VIV in the transition zone; and SCT, CDAO, and TLA in the lake zone. Anderson *et al.* (1986) described the surficial geologic formations of these stations as very soft soil (clay) for SCT and CDAO both in the lake zone, soft soil for VIV at the transition zone, and hard soil for TAC and rock (basalt) for UNAM, both in the hills zone. The other stations that recorded the 2017 event are listed in Table 1.

The 1985 recorded acceleration data from SCT and UNAM are integral in describing the main culprit (frequency content and amplification) responsible for the extensive structural damage in this event. As such, these stations best symbolize amplification in the Mexico City lake zone. Sample 1985 event acceleration records and corresponding response spectra from SCT (1985 ID), UNAM, VIV, and CDA are shown in Figure 4 (adopted from Anderson *et al.*, 1986). Design spectra from the code in effect in 1985 have been superimposed on the response spectra for comparison (Anderson *et al.*, 1986). These time histories clearly depict the amplified motions (e.g., at SCT when compared to UNAM). The SCT response spectra in Figure 4 clearly define a 2-s (0.5-Hz) resonating site period (frequency) (Mena *et al.*, 1985). It is fair to say that after the 1985 event, the response spectrum of 1985 SCT accelerations became a symbol of the amplification and resonating lakebed site period. Furthermore, station SCT (of 1985 but currently known to be the same as SCT2 station) is also important because it was close to the (Secretaria de Comunicaciones y Transportes—Ministry of Telecommunication and Transportation) building that was severely damaged in 1985. Upper floors of the building collapsed; two photos of the collapsed top floors of the SCT building are seen in Figure 5. This is notable because these motions were recorded from an event that originated ~400 km away (Fig. 1). It has been reported (but not confirmed) that the SCT building sustained extensive damage during the 2017 event as well and is under consideration to be razed.

After the 1985 mainshock, the USGS, in collaboration with Mexican scientists, deployed temporary data loggers at existing strong-motion stations and additional new temporary stations shown in Figure 2 (USA, SFO, and TLA). In an earlier study, spectral ratios with respect to UNAM station for strong and weak motions are provided by Çelebi *et al.* (1987a) and are not repeated herein. Those spectral ratios confirmed the significant amplification of motions and the resonating periods (frequencies) that are also seen in the response spectra of Figure 4 (Anderson *et al.*, 1986). As stated before, these factors caused extensive damage and loss of life and property (Stone *et al.*, 1987).

Purpose of This Study

In this study, we analyze the spectral ratios computed from strong-motion data recorded by several stations in Mexico City during the 19 September 2017 **M** 7.1 Puebla-

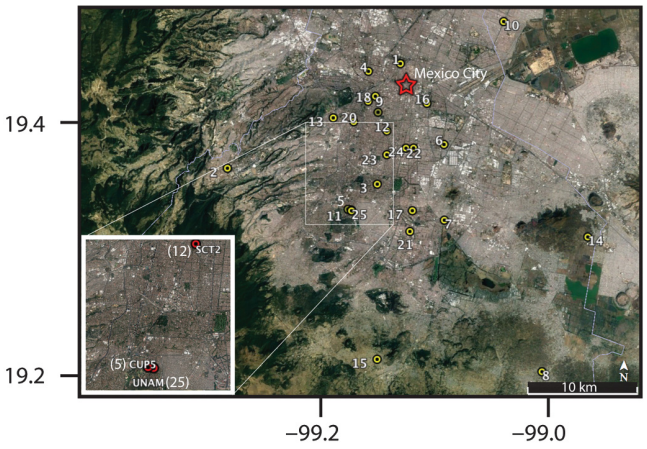

Figure 6. Google Earth Map of Mexico City with strong-motion stations used in this study, that recorded the earthquake on 19 September 2017 (yellow circles with station numbers labeled). (Inset) Stations SCT, CUP5, and UNAM are highlighted in red. The white box on main map shows the area in the inset.

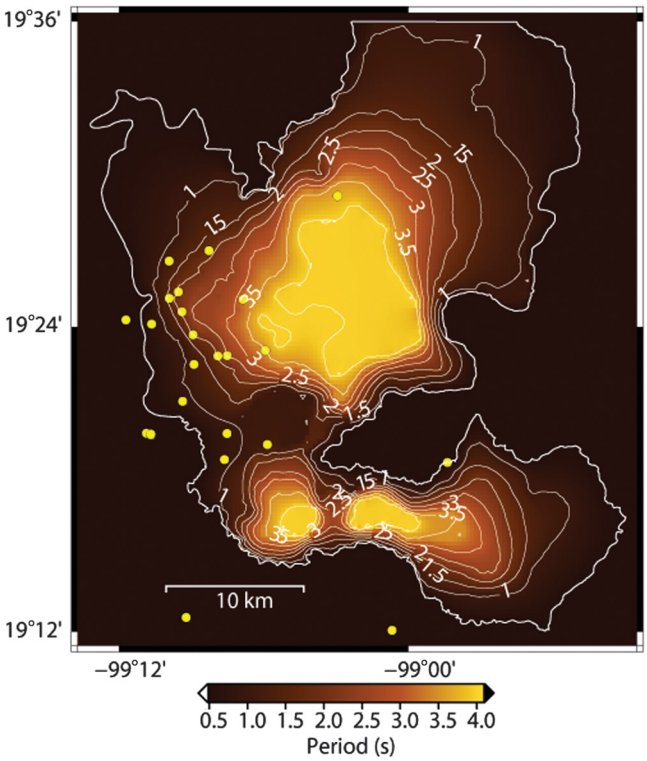

Figure 7. Map showing predominant periods in the different zones (digitized by authors using the zoning map from the Mexican seismic design code of 2004). This map is used in this article to compare periods from the code with those from strong-motion data of 2017 earthquake. Stations included in this study are shown as yellow circles.

Morelos earthquake. With these data, we aim to identify the predominant frequencies at select sites. When applicable, we compare these frequencies and spectral ratios with observed predominant frequencies from the 1985 earthquake. We also compare the frequencies and spectral ratios we compute with the current site periods (frequencies) from the seismic zoning map of Mexico City (Mexican Seismic Design Code, 2004). The scope of the article does not include tectonics, seismicity, earthquake damage reconnaissance, or assessment.

2017 Earthquake Data, Sources, and Organization

Figure 6 shows a Google Earth map with the locations of the stations in Mexico City that recorded the 2017 Puebla-Morelos earthquake. These stations are operated by the Institute of Engineering's (IINGEN) strong ground motion network of the seismic instrumentation unit within the Engineering Seismology Laboratory of the UNAM and Centro de Instrumentación y Registro Sísmico (CIRES). In this figure, we show only stations from which data were available to us and are used in this study. It should be noted that there may be more stations that recorded the earthquake.

Figure 7 is a map showing predominant periods in the different zones (digitized by authors using a similar map in the Mexican seismic design code of 2004). We will use this map to compare site periods from the code (obtained by interpolation of this map) with those site periods from strong-motion data of the 2017 earthquake computed by spectral ratios.

In Table 2, identification of stations, their coordinates, site classes, and particulars (original record length, number of points [npts], and sampling period [Δt], which is 1/sampling rate). As shown in Table 2, there is not a common record length or Δt for all of the dataset. It was noted that even for a few stations, the record lengths varied. Therefore, both the lengths of the records and Δt were standardized for all data used. This was necessary to obtain an identical length for each channel of each station and to achieve identical frequency vectors and sampling frequency (Δf). Hence, we chose a record length of 260 s and Δt of 0.01 s for all data. We accomplished this by carefully padding short (records <260 s) or chopping excess parts of records longer than 260 s. No portion of the actual earthquake time series data was truncated in the process.

Because the original lengths of the records are neither standard nor necessarily long, we did not discuss the now well-known long-duration records generated by deep basin and soft surface layers. However, such characteristics have been studied in detail by Kawase and Aki (1989) and Flores-Estrella *et al.* (2007), who presented a comprehensive review of studies on the Mexico City basin and rightly stated that the 1985 earthquake pointed to the importance of basin-site effects and that the 1985 earthquake records revealed large amplifications and long durations in the lake zone of Mexico City. Iida and Kawase (2004) reach similar conclusions by studying records from a borehole. Lermo and Chávez-García (1993, 1994) showed that microtremors show good reliability compared with those using strong motions. Other notable studies on these and similar topics related to horizontal to vertical (H/V) studies with microtremors and earthquakes include but are not limited to Kawase *et al.* (2011, 2014), and Chávez-García *et al.* (1995).

Table 2
Data Information

UNAM IINGEN Stations							
			Coordinates		Original		
This Study	Site Class (2004 Code)	Station Name	Longitude (°W)	Latitude (°N)	Δt*	Number of Points	Record Length (s)
1	IIIb	CCCL	−99.1379	19.4498	0.01	61849	615
2	I	CJVM	−99.2850	19.3616	0.01	E(10516] N[10065] Z[10298]	E[105.15 s] N[100.60 s] Z[103 s]
3	II	COVM	−99.1561	19.3511	0.01	26001	260
4	II	CTVM	−99.1655	19.4430	0.01	26001	260
5	I	CUP5	−99.1811	19.3302	0.01	41181	411.8
6	IIId	ICVM	−99.0990	19.3845	0.01	26001	260
7	IIIa*	LEAC	−99.0976	19.3228	0.005	68491	342.45 s
8	I	MPVM	−99.0114	19.2010	0.01	26001	260
9	IIIb	PCJR	−99.1591	19.4228	0.01	38791	387.9
10	IIId	PISU	−99.0490	19.4857	0.01	38891	388.9
11	I	PZIG†	−99.1780	19.3290	0.01	E[14505] N[14460] Z[14624]	145.04 s 144.59 s 146.23 s
12	IIIb	SCT2	−99.1489	19.3947	0.01	31591	315.9 s
13	I	TACY	−99.1953	19.4045	0.005	46891	234.45 s
14	I	THVM	−98.9732	19.3110	0.01	26001	260 s
15	I	TLVM	−99.1537	19.2094	0.01	26001	260 s
16	IIId	VRVM	−99.1144	19.4179	0.01	26001	260 s
CIRES Stations							
17	II‡	CH84	−99.1254	19.3300	0.01	33860	338.6
18	IIIb	CI04	−99.1566	19.4098	0.01	60000	600.0
19	IIIb	CI05	−99.1653	19.4186	0.01	32901	329.0
20	II	ES57	−99.1775	19.4017	0.01	28220	282.2
21	II	JC54	−99.1272	19.3130	0.01	35280	352.8
22	IIIb	PE10	−99.1318	19.3809	0.01	35260	352.6
23	IIIa	SI53	−99.1483	19.3753	0.01	38660	386.6
24	IIIc	VM29	−99.1253	19.3811	0.01	32901	329.0
25§	I	UNAM	−99.1780	19.3296	0.01	26001	260

Data characteristics are standardized to length of 260 s for each station and channel and with $\Delta t = 0.01$ s (100 samples per second) and reduced to or padded to 26001 points. LEAC could be either IIIa or IIIb so it is hence accepted here as IIIa. CIRES, Centro de Instrumentación y Registro Sísmico; UNAM, Universidad Nacional Autonoma de Mexico; IINGEN, Institute of Engineering.

*Delta Time (sampling rate).

†Note the short length of PZIG.

‡CH84 GEER (2017) identifies as II but could be IIIa also; hence accepted as II. All acceleration time history units are standardized to m/s/s units.

§UNAM operated station.

Data Analyses: Spectral Ratios

After standardization (as defined earlier) of the acceleration data, we compute amplitude spectra of each channel of all stations and then smoothed them using the Hanning window function in MATLAB (Mathworks, 2017). Spectral ratios are computed using the transfer function relationship

$$R_{ij}(f) = A_{ij}(f)/A_{\mathrm{ref},j}(f), \quad (1)$$

in which $A_{ij}(f)$ is the jth component of the smoothed amplitude spectrum at recording station i and similarly, $A_{\mathrm{ref},j}(f)$ is the jth component of the smoothed amplitude spectrum at the reference recording station. This relationship, also known as horizontal to horizontal (H/H) ratio, is valid assuming the differences in distance between the recording station i and reference station is negligible compared with an overall distance of ∼106 km of the reference station from the epicenter (Fig. 1). The background of such quantification of amplifications of motions as represented by spectral ratios $R_{ij}(f)$ is discussed in detail by Borcherdt (1970, 1976), Gibbs and Borcherdt (1974), Rogers *et al.* (1984), and Borcherdt and Glassmoyer (1992).

In addition to the classic spectral ratio method $R_{ij}(f)$, we also use H/V ratios, more widely known as Nakamura's method (Nakamura, 1989, 2008). This method is normally used when there are no suitable reference station data that can be used to compute $A_{\mathrm{ref},j}(f)$ in equation (1). As seen later, we successfully applied this method for the data from zones II and III.

Both the H/H and H/V methods have been extensively studied or tested in the past using microtremor or strong-shaking earthquake motions by numerous researchers including some referenced earlier as well as Lermo and Chávez-García (1993) and Flores-Estrella *et al.* (2007) for Mexico City and related data. Satoh, Fushimi, and Tatsumi (2001) and Satoh, Kawase, and Matsushima (2001) carried out similar studies using Japanese data. Salinas *et al.* (2014) studied low-amplitude and strong-shaking earthquake data from different sources recorded at Cibeles station in Mexico City in the area of heavy damage from the 1985 earthquake. They used diffuse

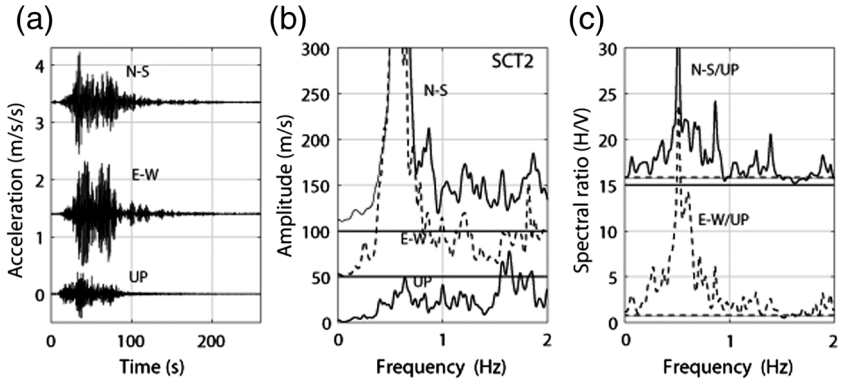

Figure 8. For station SCT2 in zone IIIb, (a) north–south, east–west, and vertical mainshock acceleration time histories; (b) amplitude spectra computed from accelerations; and (c) spectral ratios using H/V of amplitude spectra.

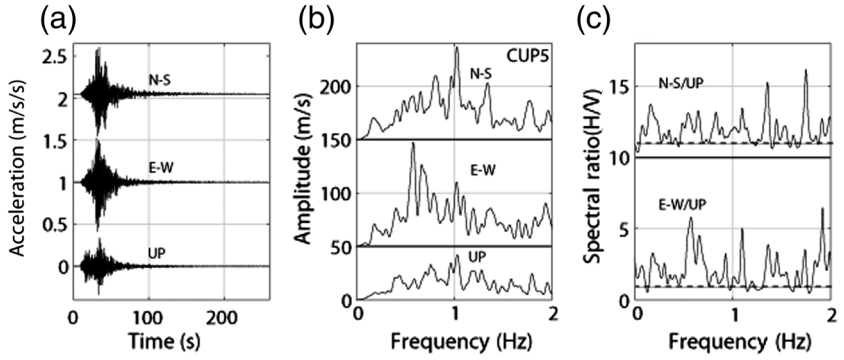

Figure 9. For station CUP5 in zone I, (a) north–south, east–west, and vertical mainshock acceleration time histories; (b) amplitude spectra computed from accelerations; and (c) spectral ratios using H/V of amplitude spectra.

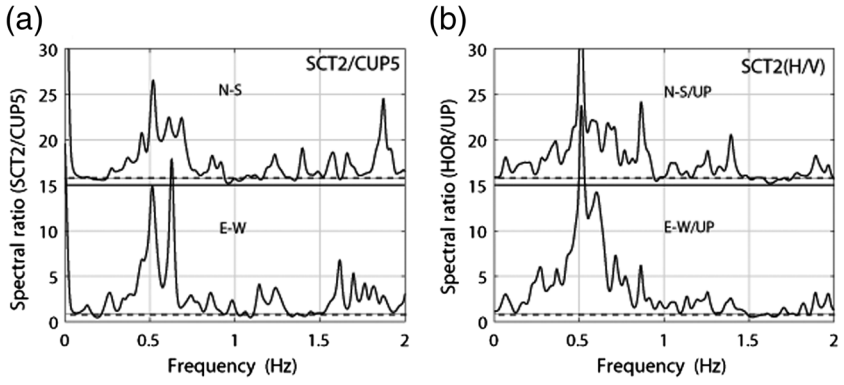

Figure 10. Comparison of (a) spectral ratios of station SCT2 (zone IIIb) with respect to station CUP5 (zone I) with (b) spectral ratios computed using H/V method only for station SCT2 amplitude spectra. The peak that appears around 0 Hz is due to numerical computation, in which the denominator is a very small number.

field theory to obtain H/V ratios and interpreted them and identified the structure. For the sake of brevity, we will not present time histories or amplitude spectra except for a couple of sample cases to demonstrate both methods.

It is imperative to state that eight stations (out of 25 in Table 1) are in zone I. Theoretically, any one of the eight stations could be used to compute $A_{\text{ref},j}(f)$ in equation (1). But before UNAM data were available, we started using CUP5 (a station very close to UNAM station; see Fig. 6). Hence, all spectral ratio computations herein are with respect to CUP5 for $A_{\text{ref},j}(f)$. Nonetheless, we validated the computations with UNAM and other relevant data for this purpose. The results, not presented here, did not change.

Sample Computations for SCT2 and CUP5 Using Two Methods

In Figure 8, for station SCT2 records in zone IIIb, we show (1) mainshock acceleration time histories in north–south, east–west, and vertical directions, (2) amplitude spectra of the accelerations, and (3) spectral ratio (H/V) for SCT2. It is noted that SCT2 is the same as the 1985 SCT station. The H/V spectral ratios clearly indicate that the dominant frequency (period) of SCT2 is ~0.5 Hz (2 s), similar to those in the 1985 response spectra, as depicted in Figure 4.

In Figure 9, we repeat the same process for CUP5 (of zone I): (1) time histories, (2) amplitude spectra, and (3) spectral ratios (H/V). As expected, there is no highly dominant frequency within the 0–2 Hz window.

Next, in Figure 10a, we compute $R_{ij}(f)=A_{ij}(f)/A_{\text{ref},j}(f)$ for SCT2 $[A_{ij}(f)]$ and CUP5 $(A_{\text{ref},j}(f))$ as the denominator. Figure 9b is identical to Figure 8c in order to compare the two methods. It is clear that the comparison is excellent, and both methods yield the dominant ~0.5 Hz site frequency for SCT2. This is a clear indication of the applicability of the H/V method for the motions recorded in Mexico City.

Spectral Ratios for Zone II

We repeat the comparison of $R_{ij}(f) = A_{ij}(f)/A_{\text{ref},j}(f)$ with H/V spectral ratios for only data from five zone II stations identified in Table 2. Figure 11a, and 11b shows five zone II stations spectral ratios computed in the north–south and east–west directions, respectively, using $R_{ij}(f) = A_{ij}(f)/A_{\text{ref},j}(f)$ with CUP5 as the denominator and similarly, Figure 11c, and 11d spectral ratios using the H/V method. At the top of each frame, an average of the five spectral ratios is shown. This figure indicates that the spread of zone II site frequencies (periods) are between ~0.7 and 1.1 Hz (~0.91–1.43 s), consistent for both methods. Varia-

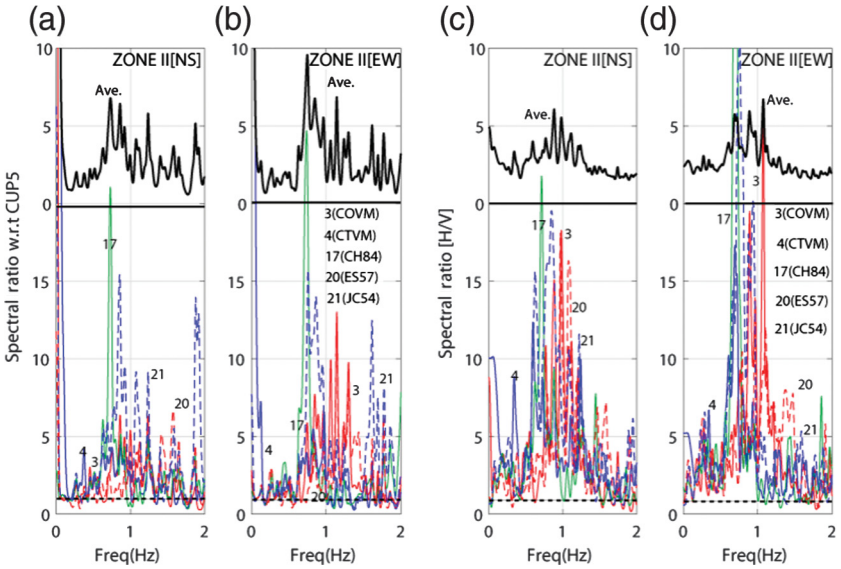

Figure 11. For five zone II stations, (a) north–south and (b) east–west spectral ratios computed using $R_{ij}(f) = A_{ij}(f)/A_{\mathrm{ref},j}(f)$ with station CUP5 as the denominator and similarly (c,d) spectral ratios using H/V method. At top part of each frame, an average of the five spectral ratios is also shown.

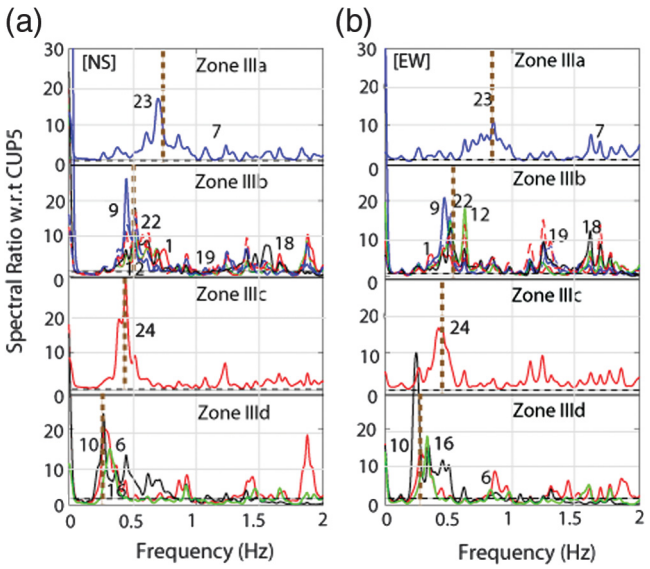

Figure 12. Spectral ratios computed with respect to station CUP5 as the denominator in all of the four zone III accelerations recorded in (a) north–south and (b) east–west directions of the stations identified by the numbering in Table 2. Dashed vertical lines are intended to depict the changing trend of frequencies from zone IIId to IIIa.

tions of site frequencies from one station to the next can be attributed to the variation of depth and log of each location.

At the top of each frame in Figure 11, we present an average of the five spectral ratios within that frame. The averages also confirm frequencies (periods) of ~0.7–1.1 Hz (~0.91–1.43 s).

Spectral Ratios for Zone III

Following the same process in Figures 12 and 13, we compare the spectral ratios by both methods individually for the stations within each of the four zone III subzones in Table 2. The number of stations in each of the subgroups varies.

Figure 12 shows $R_{ij}(f) = A_{ij}(f)/A_{\mathrm{ref},j}(f)$ with CUP5 as the denominator in all of the zone III spectral ratio versus frequency curves computed from accelerations recorded in (1) north–south and (2) east–west directions of the stations (identified by the numbering in Table 2). What is clear in each of the frames in Figure 12a,b for both north–south and east–west directions is the clear trend in increasing dominant frequency from zone IIId to zone IIIa of the zoning map (Figs. 3b and 7). For example, for zone IIId, f (or T) is ~0.25 Hz (~4.0 s), and for zone IIIa, f or T is ~0.65–0.8 Hz (~1.25–1.54 s). There is small variation between zones IIIc and IIId (e.g., f or T is ~0.8–1.0 Hz [~1.0–1.25 s]).

Similarly, Figure 13 shows the spectral ratio versus frequency curves computed by the H/V method from accelerations recorded in (1) north–south and (2) east–west directions of the stations (identified by the numbering in Table 2). The trend and site frequencies or ranges of frequencies are similar to those observed in Figure 12.

Summary of Results, Discussion, and Conclusions

Spectral ratios computed using accelerations recorded at multiple stations in Mexico City during the 19 September 2017 earthquake allow identification of site frequencies (periods). In this study, spectral ratios computed by two methods (R_{ij} and H/V) are similar. In Table 3, we summarize the results of this study and compare the site frequencies (periods) obtained by peak picking of spectral ratios using both methods (for zone II and zones IIIa, b, c, and d) with those interpolated from the predominant site period map presented in Figure 7, which is modified from the 2004 seismic design code zoning maps currently in effect in Mexico City. Because of the variations of depth and geologic formations at each station location, the variations of frequencies (periods) are justified. However, there is a clear trend, particularly for subdivisions of zone III, that indicate, as expected, showing an increase in computed frequencies from accelerations recorded at zone IIId stations to those at zone IIIa. This is consistent and justified because shear-wave velocities vary between depths of 10 and 60 m within zone III (Table 4). The differences may be attributed to (1) interpolation from the maps or (2) peak picking of the frequencies from ratios (or both).

Based on Table 3, we plot frequencies obtained from the 2004 seismic design code zoning map against those identified from the two spectral ratio methods explained earlier. Figure 14 shows the comparison; the agreement is strong.

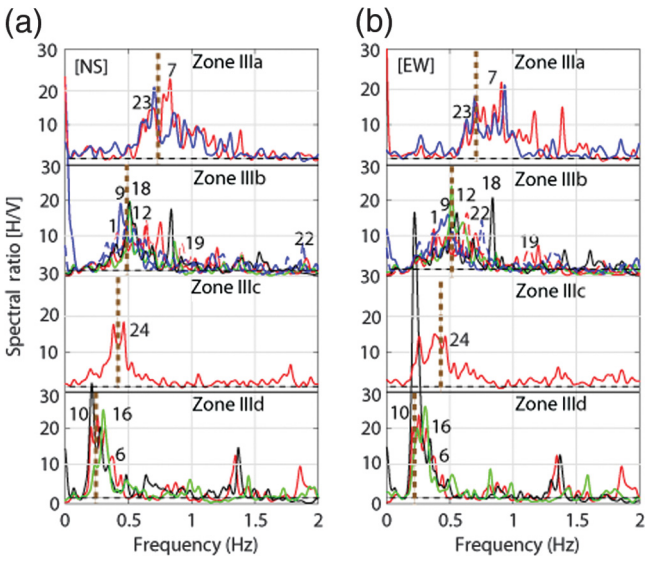

Figure 13. Spectral ratios computed by the H/V method from accelerations recorded in (a) north–south and (b) east–west directions for all of the four zone III stations identified by the numbering in Table 2. Dashed vertical lines are intended to depict the changing trend of frequencies from zone IIId to IIIa.

In Table 4, we further summarize the results by providing the range of frequencies and soil depth (for zone III as shown in the 2004 Mexican seismic design code). It is clear that the variations observed in Figure 4 are also attributable to the variation of soil depth—a factor that is significant. Variation of shear-wave velocity (V_S) with depth at different stations, although not known, may affect the results as well.

We conclude that predominant site frequencies (periods) identified from spectral ratios computed for ground motions recorded in Mexico City during the mainshock of the 19 September 2017 **M** 7.1 Puebla-Morelos earthquake are in good agreement with those indicated in the site period map of the 2004 Mexican seismic design code. The agreement is best for zone III and relatively good for zone II stations. The differences can be attributed to one or a combination of several factors, including (1) interpolation errors from the maps, (2) peak picking errors of the frequencies from spectral ratios, (3) variations of depth, (4) associated V_S values of the underlying soil at different locations, and (e) differences in H/V to H/H (soil/rock) ratios. Most important, the difference is most likely due to physical differences between H/H spectral ratios computed with respect to a reference station and H/V spectral ratios computed with respect to vertical motion at the same station. Furthermore, we conclude that the H/V method can be reliably used with data from Mexico City.

Although the correlation of the predominant zoning site periods of the observed data and those included in the maps of the 2004 seismic design code are satisfactory, it is hereby emphasized that such agreement does not at all imply that the spectral levels in the code are sufficient or not for earthquake-resistant design of buildings in the lake zone of Mexico City. Additional studies to this effect are recommended.

Table 3
Summary Table of Site Frequencies Obtained from Spectral Ratios and Digitized Zoning Map

Station			f (Hz) R_{ij}		f (Hz) H/V		Zoning Map	
Number	Label	Zone	North–South	East–West	North–South	East–West	T (s)	f (Hz)
1	CCCL	IIIb	0.35	0.35	0.4	0.4	1.84	0.54
2	CJVM	I						
3	COVM	II	0.85	1	0.9	1	0.80	1.26
4	CTVM	II	0.7	0.8	0.7	0.7	1.19	0.84
5	CUP5	I					0.50	2.00
6	ICVM	IIId	0.3	0.3	0.25	0.25	3.50	0.29
7	LEAC	IIIa	0.7	0.85	0.7	0.7	1.04	0.96
8	MPVM	I					0.50	2.00
9	PCJR	IIIb	0.45	0.45	0.42	0.47	2.03	0.49
10	PISU	IIId	0.27	0.25	0.24	0.24	3.67	0.27
11	PZIG+	I					0.50	2.00
12	SCT2	IIIb	0.52	0.47	0.51	0.52	2.00	0.50
13	TACY	I					0.50	2.00
14	THVM	I					0.51	1.95
15	TLVM	I					0.50	2.00
16	VRVM	IIId	0.32	0.33	0.28	0.29	3.27	0.31
17	CH84	II	0.75	0.75	0.75	0.75	0.92	1.08
18	CI04	IIIb	0.5	0.52	0.51	0.56	2.09	0.48
19	CI05	IIIb	0.44	0.52	0.52	0.51	1.64	0.61
20	ES57	II	0.8	0.8	0.8	0.8	0.72	1.39
21	JC54	II	0.85	0.85	0.8	0.8	0.89	1.13
22	PE10	IIIb	0.35	0.51	0.51	0.56	2.05	0.49
23	SI53	IIIa	0.7	0.85	0.7	0.7	1.20	0.83
24	VM29	IIIc	0.44	0.45	0.45	0.45	2.54	0.39
25	UNAM	I					0.50	2.00

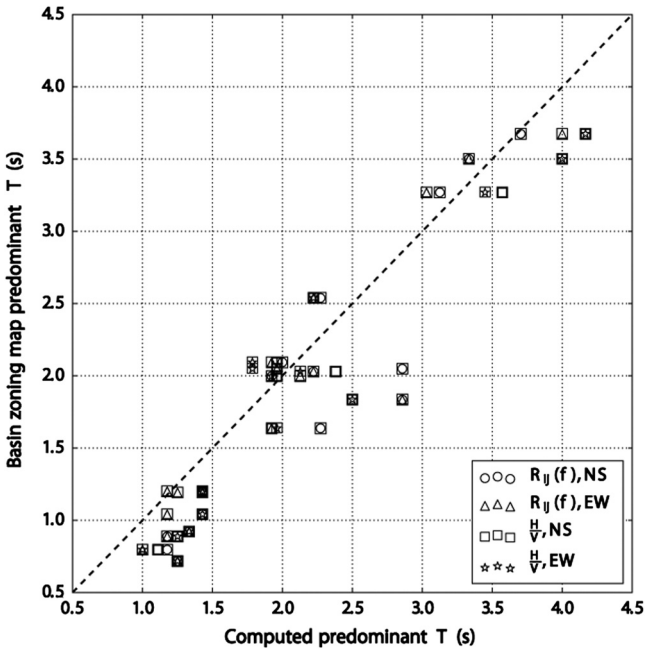

Figure 14. Comparison of predominant site periods: zoning map of 2004 Code versus those determined from R_{ij} and H/V ratios. The diagonal dashed line is inserted to provide a 1:1 view of relative variation of T.

Data and Resources

The data used in this work were kindly provided by the Red Sísmica del Valle de México (RSVM) of the Servicio Sismológico Nacional (SSN, Mexican National Seismological Service); station maintenance, data acquisition, and distribution are thanks to its personnel. Financial support is provided by Consejo Nacional de Ciencia y Tecnología (CONACYT, National Council for Science and Technology), Universidad Nacional Autónoma de México (UNAM, National Autonomous University of Mexico), and Gobierno de la Ciudad de México (Government of Ciudad de México). Instrumentation and processing work are courtesy of the Seismic Instrumentation Unit at the Institute of Engineering of the National Autonomous University of Mexico (UNAM, www.iingen.unam.mx, last accessed April 2018). The information about the Ayutla, Mexico, earthquake is available at https://earthquake.usgs.gov/earthquakes/eventpage/us2000ar20#executive (last accessed January 2018). Photos are by M. Çelebi and are found in (a) https://library.usgs.gov/photo/#/tem/51dc314ae4b0f81004b79eec, and (b) https://library.usgs.gov/photo/#/item/51dc314ce4b0f81004b79eee (last accessed August 2018). Center for Engineering Strong Motion Data are available at www.strongmotioncenter.org (last accessed April 2018). The information about the 1985 Mexico earthquake is available at https://www.nist.gov/publications/engineering-aspects-september-19-1985-mexico-earthquake-nbs-bss-165 and http://ws680.nist.gov/publication/get_pdf.cfm?pub_id=908821 (last accessed April 2018).

Acknowledgments

Cory Hurd and Luke Blair, both at the U.S. Geological Survey, graciously helped produce some of the maps. Roger Borcherdt and Alex Grant kindly provided helpful and constructive reviews of the article. Monica Erdman conducted in-depth editing. The authors thank the two anonymous reviewers as well as the associate editor for constructive comments.

These preliminary strong ground-motion data are generated as received. The records belong to Universidad Nacional Autonoma de Mexico (UNAM's) Institute of Engineering and cannot be redistributed in original, processed, or modified formats. Any use of trade, firm, or product names is for descriptive purposes only and does not imply endorsement by the U.S. Government.

References

Anderson, J. G., P. Bodin, F. N. Brune, J. Prince, S. K. Singh, R. Quass, and M. Onate (1986). Strong ground motion from the Michoacan, Mexico earthquake, *Science* **233,** no. 4768, 1043–1049.

Arroyo, D., M. Ordaz, E. Ovando-Shelley, J. Guasch, J. Lermo, C. Perez, L. Alcantara, and M. Ramírez-Centeno (2013). Evaluation of the change in dominant periods in the lake-bed zone of Mexico City produced by ground subsidence through the use of site amplification factors, *Soil Dynam. Earthq. Eng.* **44,** 54–66.

Bard, P. Y., and M. Bouchon (1980). The seismic response of sediment-filled valleys. Part 1, The case of incident SH waves, *Bull. Seismol. Soc. Am.* **70,** no. 4, 1263–1286.

Borcherdt, R. D. (1970). Effects of local geology on ground motion near San Francisco Bay, *Bull. Seismol. Soc. Am.* **60,** 29–61.

Borcherdt, R. D. (1976). Effects of local geological conditions in the San Francisco Bay Region on ground motions and intensities of the 1906 earthquake, *Bull. Seismol. Soc. Am.* **66,** 467–600.

Borcherdt, R. D., and G. Glassmoyer (1992). On the characteristics of local geology and their influence on ground motions generated by the Loma Prieta earthquake, in the San Francisco Bay region, California, *Bull. Seismol. Soc. Am.* **82,** 603–641.

Çelebi, M., C. Dietel, J. Prince, C. Dietel, M. Onate, and G. Chavez (1987a). The culprit in Mexico City—Amplification of motions, *Earthq. Spectra* **3,** no. 2, 315–328.

Çelebi, M, C. Dietel, J. Prince, C. Dietel, M. Onate, and G. Chavez (1987b). Site amplification in Mexico City (determined from 19 September 1985 strong-motion records and from recording of weak motions),

Table 4
Summary of Range of Soil Depth and Site Frequencies (Periods) According to 2004 Mexican Seismic Design Code and This Study

	2004 Code Designated Zones II and III				
	II	IIIa	IIIb	IIIc	IIId
Depth h (m) 2004 code	–	10–60m			
2004 code f(Hz)/T (s)	–	0.29–0.67 (1.5–3.5)			0.25–0.67 (3.5–4.0)
This study f(Hz)/T (s)	0.7–1.1 Hz (1.25–1.54s)	0.65–0.80 (1.25–1.54)	0.8–1.0 (1.0–1.25)		0.25 (4.00)

in *Ground Motion and Engineering Seismology*, A. S. Cakmak (Editor), 141–152.

Chávez-García, F. J., and P. Y. Bard (1994). Site effects in Mexico City eight years after the September 1985 Michoacan earthquakes, *Soil Dynam. Earthq. Eng.* **13,** no. 4, 229–247.

Chávez-García, F. J., and L. Salazar (2002). Strong motion in central Mexico: A model based on data analysis and simple modeling, *Bull. Seismol. Soc. Am.* **92,** no. 8, 3087–3101.

Chávez-García, F. J., J. Ramos-Martínez, and E. Romero-Jiménez (1995). Surface-wave dispersion analysis in Mexico City, *Bull. Seismol. Soc. Am.* **85,** 1116–1126.

Cruz-Atienza, V. M., J. Tago, J. D. Sanabria-Gómez, E. Chaljub, V. Etienne, J. Virieux, and L. Quintanar (2016). Long duration of ground motion in the paradigmatic valley of Mexico, *Sci. Rep.* **6,** 38,807.

Flores-Estrella, H. F., S. Yussim, and C. Lomnitz (2007). Seismic response of the Mexico City basin: A review of twenty years of research, *Nat. Haz.* **40,** 357–372, doi: 10.1007/s11069-006-0034-6.

Geotechnical Extreme Events Reconnaissance (GEER) Association (2017). Geotechnical engineering reconnaissance of the 19 September 2017 M_w 7.1 Puebla-Mexico City earthquake, in *GEER Rept. No. GEER-055A, Version 1.0*, Mayoral, J. M., T. C. Hutchinson, and K. W. Franke (Editors), 92 pp., doi: 10.18118/G6JD46.

Gibbs, J. F., and R. D. Borcherdt (1974). Effects of local geology on ground motion in the San Francisco Bay region, California—A continued study, *U.S. Geol. Surv. Open-File Rept. 74-222*.

Iida, M., and H. Kawase (2004). A comprehensive interpretation of strong motions in the Mexican Volcanic Belt, *Bull. Seismol. Soc. Am.* **94,** no. 2, 598–618.

Kawase, H. (2003). Site effects on strong ground motions, in *Part B of International Handbook of Earthquake and Engineering Seismology*, W. H. K. Lee, H. Kanamori, P. Jennings, and C. Kisslinger (Editors), Academic Press (Elsevier Science) for International Association of Seismology and Physics of The Earth's Interior (IASPEI), Cambridge University Press, Cambridge, United Kingdom, 1013–1030.

Kawase, H., and K. Aki (1989). A study on the response of a soft basin incident *S*, *P*, and Rayleigh Waves with special reference to Mexico City, *Bull. Seismol. Soc. Am.* **79,** 1361–1382.

Kawase, H., F. Nagashima, S. Matsushima, and F. J. Sánchez-Sesma (2014). Application of horizontal to vertical (H/V) spectral ratios for both microtremors and earthquake motions based on the diffuse field theory, *10th U.S. National Conference on Earthquake Engineering Frontiers of Earthquake Engineering (10NCEE)*, Anchorage, Alaska, 21–25 July 2014.

Kawase, H., F. J. Sánchez-Sesma, and S. Matsushima (2011). The optimal use of horizontal-to-vertical spectral ratios of earthquake motions for velocity inversions based on diffuse-field theory for plane waves, *Bull. Seismol. Soc. Am.* **101,** no. 5, 2001–2014, doi: 10.1785/0120100263.

Lermo, J., and J. F. Chávez-García (1993). Site effect evaluation using spectral ratios with only one station, *Bull. Seismol. Soc. Am.* **83,** 1574–1594.

Lermo, J., and J. F. Chávez-García (1994). Are microtremors useful in site response evaluation? *Bull. Seismol. Soc. Am.* **84,** no. 5, 1350–1364.

Mathworks (2017). *MATLAB and Toolboxes*, The Mathworks, Inc., South Natick, Massachusetts.

Melgar, D., X. Pérez-Campos, L. Ramirez-Guzman, Z. Spica, V. H. Espíndola, W. C. Hammond, and E. Cabral-Cano (2018). Bend faulting at the edge of a flat slab: The 2017 M_w 7.1 Puebla-Morelos, Mexico earthquake, *Geophys. Res. Lett.* **45,** 2633–2641.

Mena, E., R. Quaas, J. Prince, D. Almora, and P. Perez (1985). Accelerograma en el Centro Scope de Comunicaciones y Transportes, Sismo del 19 de 1985, *Informe IPS-lOB, 200985 Instituto de Ingenieria UNAM* (in Spanish).

Mendoza, C., and S. H. Hartzell (1989). Slip distribution of the 19 September 1985 Michoacan, Mexico, earthquake: Near-source and teleseismic constraints, *Bull. Seismol. Soc. Am.* **79,** no. 3, 655–669.

Mexican Seismic Design Code (2004) *Complimentary Technical Norms for Seismic Design* (in Spanish Normas Tecnicas Complementarias Para Diseno Por Sismo). (also see [RCDF, Reglamento de Construcciones para el Distrito Federal] (2004). Administración Pública del Distrito Federal, Jefatura de Gobierno, Normas Técnicas Complementarias para el Diseño por Sismos, México).

Nakamura, Y. (1989). A method for dynamic characteristics estimation of subsurface using microtremor on the ground surface, *Q.Rep. Railway Tech. Res. Inst. (Japan)* **30,** 25–30.

Nakamura, Y. (2008) On the H/V spectrum, *The 14th World Conference on Earthquake Engineering*, Beijing, China, 12–17 October 2008, 1–10.

Rogers, A. M., R. D. Borcherdt, P. A. Covington, and D. M. Perkins (1984). A comparative ground response study near Los Angeles using recordings of Nevada nuclear tests and the 1971 San Fernando earthquake, *Bull. Seismol. Soc. Am.* **74,** no. 5, 1925–1949.

Salinas, V., F. Luzón, A. García-Jerez, F. J. Sánchez-Sesma, H. Kawase, S. Matsushima, M. Suarez, A. Cuellar, and M. Campillo (2014). Using diffuse field theory to interpret the H/V spectral ratio from earthquake records in Cibeles seismic station, Mexico City, *Bull. Seismol. Soc. Am.* **104,** no. 2, 995–1001, doi: 10.1785/0120130202.

Sánchez-Sesma, F., S. Chávez-Pérez, M. Suarez, M. A. Bravo, and L. E. Pérez-Rocha (1988). The Mexico earthquake of September 19, 1985—On the seismic response of the Valley of Mexico, *Earthq. Spectra* **4,** no. 3,569–589.

Satoh, T., M. Fushimi, and Y. Tatsumi (2001). Inversion of strain-dependent nonlinear characteristics of soils using weak and strong motions observed by borehole sites in Japan, *Bull. Seismol. Soc. Am.* **91,** 365–380, doi: 10.1785/0120000049.

Satoh, T., H. Kawase, and S. Matsushima (2001). Differences between site characteristics obtained from microtremors, *S*-waves, *P*-waves, and codas, *Bull. Seismol. Soc. Am.* **91,** 313–334, doi: 10.1785/0119990149.

Shapiro, N. M., M. Campillo, A. Paul, S. K. Singh, D. Jongmans, and F. J. Sanchez-Sesma (1997). Surface-wave propagation across the Mexican Volcanic Belt and the origin of the long-period seismic-wave amplification in the Valley of Mexico, *Geophys. J. Int.* **128,** no. 1, 151–166.

Singh, S. K., and M. Ordaz (1993). On the origin of long coda observed in the lake-bed strong-motion records of Mexico City, *Bull. Seismol. Soc. Am.* **83,** no. 4, 1298–1306.

Stone, W. C., F. Y. Yokel, M. Çelebi, T. Hanks, and E. V. Leyendecker (1987). Engineering Aspects of the September 19, 1985 Mexico Earthquake, *U.S. Dept. of Commerce National Institute of Standards and Technology (NIST) Building Science Series Report Number 165*, 215 pp.

Earthquake Science Center
U.S. Geological Survey
Menlo Park, California 94025
celebi@usgs.gov
(M.Ç.)

Department of Earth Sciences
University of Oregon
Eugene, Oregon 97403
(V.J.S., D.M.)

Universidad Nacional Autónoma de México (UNAM)
Instituto de Geofísica
04510 CDMX
Mexico
luisq@igeofisica.unam.mx
(L.Q.)

Manuscript received 9 April 2018;
Published Online 11 September 2018